POLYDISPERSED SOLIDS BEHAVIOR IN A BUBBLE COLUMN

DEPARTMENT OF ENERGY, PITTSBURGH, PA.
PITTSBURGH ENERGY TECHNOLOGY CENTER

1984

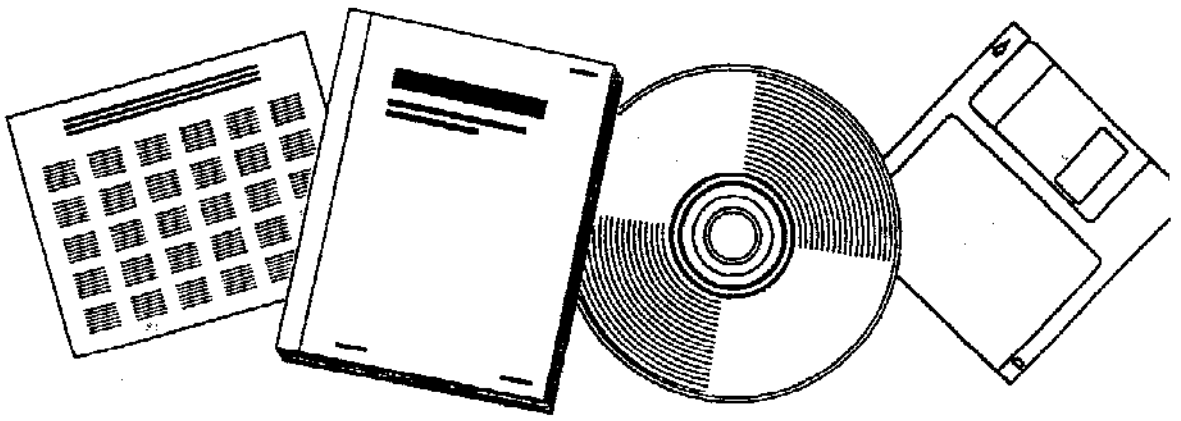

U.S. DEPARTMENT OF COMMERCE
National Technical Information Service

Introduction

The slurry bubble column reactor has increasing applications in petrochemical and coal processing [L'Homme (1979), and Chaudhari and Ramachandran (1980)]. The use of a slurry bubble column reactor is generally restricted to particle diameters less than 2.0×10^{-4}-m to satisfy the requirement of complete suspension of solids under nominal operating conditions. In most applications, the particle size in a slurry reactor are not uniform but rather have some form of a distribution. The effect of particle size distribution on the hydrodynamic behavior of a slurry bubble column has received little attention in the literature [Reilly et al. (1982)].

Particle behavior in a bubble column reactor is influenced by the slip velocity between the solid phase and liquid phase and by the solids mixing. Previous workers have described the behavior of solids by a one-dimensional sedimentation-dispersion model [Cova (1966), and Suganuma and Yamanishi (1966)]. Several variations of the model have been proposed for steady-state conditions and have been summarized by Smith and Ruether (1984). For monodispersed solids, knowledge of the solids dispersion coefficient, relative velocities of the three phases, and solids concentration at the top or bottom of the column is required to evaluate the residence time and residence time distribution of the solids in the reactor [Cova (1966) and Yamamaka et al. (1970)]. For polydispersed solids, the solids dispersion coefficient and relative velocity between the solid and liquid phase are dependent on the distribution of particle size and/or density.

In this communication, new data are presented for polydispersed solids in bubble columns with aqueous systems. Also presented in a method for computing axial distribution of solids having a distribution of particle size. The purpose of this work is to extend the data base for dispersed solids in a bubble column to include the effect of particle size distributions which is commonly encountered in slurry bubble column reactors and to provide a reasonable approach to predict solids concentration distributions for these systems.

Experimental

A schematic diagram of the slurry bubble column apparatus is shown in Figure 1. The bubble column is a transparent acrylic cylinder having an inside diameter of 0.108-m and length of 1.94-m. Average bulk fluid temperature was measured in the center of the column with a 0.0016-m-diameter type-E thermocouple. Temperature ranged between 296°K and 300°K for all experiments. A perforated plate distributor containing 72 holes of 0.001-m-diameter was located at the bottom of the column and used to introduce the gas and slurry streams.

The liquid and gas phases were nitrogen and water, respectively. The solid phase consisted of binary and ternary mixtures of narrow-sized glass spheres. The narrow-sized solids fractions were either minus 210 μm plus 177 μm, or minus 53 μm plus 44 μm in diameter. The density of the glass spheres were either 2420 kg/m^3 or 3990 kg/m^3. All solids used in this study were specified as greater than 90 percent true spheres. Table 1 gives the operating conditions for this study.

The axial solid concentration distributions were measured at continuous gas and slurry flows operated at steady-state conditions. The gas flow rate was metered with a rotometer and the slurry flow rate was measured with a venturi meter. The slurry was pressurized with a progressive cavity pump having a synthetic rubber stator to avoid particle disintegration. Slurry velocities were maintained above the saltation velocities in the feed line. A 30-degree tapered cone section just below the distributor was employed to establish a smooth transition from feed lines to the bubble column. After steady-state conditions were established in the column (experimentally verified as requiring less than one hour for the entire range of experimental conditions), samples of the slurry were withdrawn through six sampling ports located at 0.35-m intervals along the column axis beginning at 0.054-m from the distributor plate. All six samples were obtained simultaneously with electronically actuated sample valves connected in parallel to a single switch.

The total solids concentration from slurry sampling were obtained from the measured slurry sample weight, dried solids weight, and liquid and solid densities. In addition to the total solids concentration, the solids concentration of each narrow-sized fraction was obtained from pulsed sieve analysis of the dried solids. Gas holdup was calculated from the column height and the settled slurry level in the column after sudden interruption of flows. The total mass of solids in the bubble column was calculated from the difference of the known mass of solids initially introduced into the apparatus and the mass of solids in the recirculation tank. The mass of solids in the recirculation tank was measured by stopping all flows and recovering the retained solids. The average solids concentration in the

bubble column is then calculated as the ratio of the total mass of solids in the bubble column to the volume of the slurry calculated from the slurry height after abrupt interruption of flows.

Analysis of Solids Distributions

For monodispersed particles, the solids concentration distribution in a cocurrent upward flow slurry bubble column operated at steady-state conditions appears to be well described by a one-dimensional sedimentation-dispersion model. Smith and Ruether (1984) provide the following mass balance of the solids for any axial position in the column which is a result of solids dispersion, hindered settling and convection of the solids.

$$\frac{-E_s}{L}\frac{dc_s}{dx} + \left[\frac{\bar{U}_{si}}{(1-\varepsilon g)} - \bar{\psi}_L U_p\right] C_s = \bar{U}_{si} C_s^f \qquad (1)$$

Equation (1) has been derived with the following assumptions: (1) gas hold-up is independent of axial position, (2) steady-state flow conditions, (3) the liquid fraction in the slurry, ψ_L, does not change with axial position, (4) uniformly constant particle size and density. Although the liquid fraction in the slurry does change slightly with axial position, the value of the average liquid fraction is generally very close to the actual liquid fraction anywhere in the column for a wide range of operating conditions. For the present study, the average liquid fraction was always within 7 percent of the actual liquid fraction anywhere in the column for the entire range of flow conditions.

For polydispersed particle size, a non-uniform size establishes non-uniform settling and mixing rates of the solids in the column. The larger particles tend to settle at a higher rate than the smaller particles and to preferentially concentrated near the bottom of the column. In addition to an axial concentration of solids, an axial distribution of particle size must be considered. Separating a distribution of particle size into narrow fractions allows the formulation of a mass balance on each individual narrow fraction of particle size.

$$\frac{-E_{si}}{L}\frac{dC_{si}}{dX} + \left[\frac{\bar{U}_{si}}{(1-6g)} - \bar{\psi}_L U_{pi}\right] C_{si} = U_{si} C_{si}^{\,f} \qquad (2)$$

Equation (2) represents a mass balance for the i^{th} particle size fraction in a polydispersed solids system having a solids concentration in the slurry, C_{si}, dependent on the settling and mixing rates of the i^{th} particle characteristics. The hindered settling velocity relative to the column, $\bar{\psi}_L U_{pi}$, takes into account interference of all other particles with the term $\bar{\psi}_L$, the average liquid fraction in the slurry. Integration of Equation (2) yields an expression in the following form.

$$C_{si} = C_1 + C_2 \exp\left[\frac{-(\bar{\psi}_L U_{pi} - U_{sL})LX}{E_{si}}\right] \qquad (3)$$

The constants C_1 and C_2 can be determined by consideration of the solids concentration at the bottom or top of the column using Equations (2) and (3). For C_1,

$$C_1 = -U_{sL} C_{si}^{\,f} \,/\, (\bar{\psi}_L U_{pi} - U_{sL}) \qquad (4)$$

and for C_2 in terms of the solids concentration at the bottom of the column,

$$C_2 = C_{si}^{o} + U_{sL}C_{si}^{f} \,/\, (\bar{\psi}_L U_{pi} - U_{sL}) \tag{5a}$$

or for C_2 in terms of the solids concentration at the top of the column,

$$C_2 = [C_{si}^{1} + \frac{U_{si}C_{si}^{f}}{(\bar{\psi}_L U_{pi} - U_{sL})}] \exp [\frac{(\bar{\psi}_L U_{pi} - U_{si})L}{E_{si}}] \tag{5b}$$

Combining Equations (4), (5a), and (5b) with Equation (3) gives the result of the axial solids concentration distribution for the i^{th} particle fraction from the sedimentation-dispersion model.

$$C_{si} = [C_{si}^{o} + [\frac{U_{sL}C_{si}^{f}}{(\bar{\psi}_L U_{pi} - U_{sL})}] \exp [\frac{-(\bar{\psi}_L U_{pi} - U_{sL})LX}{E_{si}}] \tag{6a}$$

$$- \frac{U_{sL}C_{si}^{f}}{(\bar{\psi}_L U_{pi} - U_{sL})}$$

$$C_{si} = [C_{si}^{1} + \frac{U_{sL}C_{si}^{f}}{(\bar{\psi}_L U_{pi} - U_{si})}] \exp [\frac{-(\bar{\psi}_L U_{pi} - U_{sL})L(X-1)}{E_{si}}] \tag{6b}$$

$$- \frac{U_{sL}C_{si}^{f}}{(\bar{\psi}_L U_{si} - U_{sL})}$$

The total solids concentration in the slurry at any given axial position is the sum of all particle fraction concentrations.

$$C_s = \sum_{i=1}^{n} C_{si} \tag{7}$$

Where the solid concentration for the i^{th} particle fraction can be expressed in terms of the sum of all particle fractions as:

$$C_{si} = \phi_i C_s \tag{8}$$

Here ϕ_i is defined as the mass fraction of the i^{th} particle fraction and the following identities are valid.

$$\sum_{i=1}^{n} \phi_i = 1 \tag{9}$$

and

$$\sum_{i=1}^{n} \frac{d\phi_i}{dX} = 0 \tag{10}$$

Combining Equation (2) with Equations (7), (8), (9), and (10) gives the expression for total solids concentration for polydispersed solids using the sedimentation-dispersion model.

$$\Sigma\left(\frac{-E_{si}\phi_i}{L}\right) \frac{dC_s}{dX} + [U_{sL} - \bar{\psi}_L \Sigma(\phi_i U_{pi})] C_s = U_{sL} C_s^{\,f} \tag{11}$$

The summation terms on the left hand side of Equation (11) are a function of axial position for polydispersed systems. For solids having a greater density than liquid, the summation term, $\Phi_i U_{pi}$, decreases with increasing axial position whereas the summation term, $\Phi_i E_{si}$, increases with increasing axial position. Equation (11) illustrates the nonlinear behavior of solids concentration with axial position for polydispersed solids systems in a slurry bubble column. Equation (6a) or (6b) combined with Equation (7) provides a solution for the axial solids concentration distribution from knowledge of the polydispersed solids size distribution, operating conditions, hindered settling velocity, and solids dispersion coefficient.

For analysis of the axial solids concentration distribution, Equation (6a) is used to predict the solids concentration, $C_{si}(X)$, with the best fit of measured solids concentration being optimized with the parameters U_{pi}, E_{si}, and C_{si}^{o}. For each computation, the six measured slurry concentrations were used and the values of the three parameters were determined to minimize the residual sum of squares between the observed and calculated solids concentration. The objective function employed was

$$F = \sum_{j=1}^{6} [C_{si}\ (\text{calculated}) - C_{si}\ (\text{observed})]_j^2 \qquad (12)$$

A search method described by Ahrendts and Baehr (1981) was used to obtain the minimum value of F. The value of F was less than 0.0001 for all experimental conditions. Empirical correlations are then developed for the parameters, U_{pi}, E_{si}, C_{si}^{o}, and C_{si}^{1} in terms of the operating variables. The

total solids concentration as a function of axial position is then determined from Equation (7) and the parameter correlations. Figure 2 shows the method of analysis for measured axial solids concentration distributions.

Results

In the following, first; empirical correlations are developed for the transport parameters, ϵ_g, U_{pi}, E_{si} and C_{si}? obtained from the method described in Figure 2. Next, the effects of several independent variables on the axial distribution of solids is given and compared with the experimental data.

Gas Holdup

Average gas holdup obtained in a slurry bubble column have been compared with several correlations in the literature [Akita and Yoshida (1973), Hikita et al. (1980), and Hughmark (1967]. The best agreement between observed and predicted gas holdup was obtained with the correlation proposed by Hughmark (1967), as given by the following expression.

$$\epsilon_g = [2 + (0.35/\bar{U}_g)\ (\rho_L \sigma_L/72)^{1/3}]^{-1} \qquad (13)$$

The maximum deviation between observed and predicted gas holdup was less than 15 percent with an average deviation of 6.7 percent. The range of gas holdup and superficial gas velocity was from 0.095 to 0.285 and 0.031 to

0.20 m/s, respectively. Liquid surface tension and density remained essentially constant at 0.072 n/m and 1000 kg/m^3, respectively.

Hindered Settling Velocity

The hindered settling velocity, U_p, for a slurry bubble column represents the slip velocity between the solid and liquid phases. The hindered settling velocities obtained in this investigation by the method shown in Figure 2 are predicted well with the correlations given by Kato et al. (1972) and Smith and Ruether (1984). These correlations predict a dependency of the hindered settling velocity on the terminal particle velocity, gas velocity, and average liquid holdup in the slurry. Since the average liquid holdup in the slurry was not varied significantly in the present investigation ($0.942<\bar{\psi}_L<0.965$), the dependency on hindered settling velocity on this variable is assumed to be the same as given by Smith and Ruether (1984). A regression analysis of the hindered settling velocity on operating variables has given the following equation:

$$U_{pi} = 1.44\, U_{ti}^{0.78}\, \bar{U}_g^{0.23}\, \bar{\psi}_L^{3.5} \qquad (14)$$

The average absolute relative deviation between the observed hindered settling velocity and that predicted from Equation (14) is 9.6 percent. The range of terminal particle velocities is from 0.002 to 0.022 m/s. Figure 3 shows the effect of gas velocity on the hindered settling velocity. Equation (14) applies to each narrow-sized fraction of solids in the slurry

bubble column having a unique terminal particle velocity. From this correlation it is evident that for polydispersed solid systems, the hindered settling velocity is little affected by particle-particle interaction and that the particles behave as well dispersed solids. A parity plot of the observed and predicted hindered settling velocities from Equation (14) is given in Figure 4.

Solids Dispersion Coefficient

Axial solids backmixing or dispersion is characteristic of slurry bubble columns and may be described in terms of a solids dispersion coefficient. The dispersion of solids has been shown to be proportional to the dispersion of liquid and to approach liquid dispersion behavior for small particle Reynolds numbers [Kato et al. (1972)]. Figure 5 shows the change in the solids dispersion coefficient for polydispersed solids with the gas velocity for several partial Reynolds numbers and illustrates the correlation given by Smith and Ruether (1984) for monodispersed solids. For the polydispersed solids system, the solids dispersion coefficient is more strongly influenced by the particle Reynolds number than for monodispersed solids. Presently, it is difficult to interpret this discrepancy between the polydispersed and monodispersed solids dispersion coefficient. It should be noted, however, that the present study has employed a perforated plate distributor whereas Smith and Ruether (1984) have employed a bubble cap distributor.

A dimensionless analysis of the solids dispersion coefficient in terms of a solids Peclet number, similar to the expression given by Smith and

Ruether (1984), has been used to correlate the dependence of the solids dispersion coefficient on operating variables. A regression analysis of the experimental data yield the following expression

$$Pe_{pi} = 6.7\ (Fr_g^6/Re_g)^{0.106}[1 + 0.15\ Re_{pi}] \qquad (15)$$

where: $Pe_{pi} = \bar{U}_g D/E_{si}$; $0.25 < Pe_{pi} < 1.3$

$Re_g = \bar{U}_g D\rho_L/\mu_L$; $3700 < Re_g < 1200$

$Fr_g = \bar{U}_g/(gD)^{1/2}$; $0.03 < Fr_g < 0.20$

$Re_{pi} = d_{pi}\rho_L U_{ti}/\mu_L$; $0.1 < Re_{pi} < 5$

A parity plot of the measured and predicted solids Peclet number is given in Figure 6. Greater than 90 percent of the solids Peclet numbers is predicted within $\pm$ 20 percent of the observed values.

Solids Concentration at Top and Bottom of Column

The solids concentration at the top of the column is related to the solids concentration at the bottom of the column for narrow-sized particles by Equation (6a).

$$C_{si}^{1} = [C_{si}^{o} + \frac{U_{sL}}{(\bar{\Psi}_L U_{pi} - U_{sL})}] \exp\ [\frac{-(\bar{\Psi}_L U_{pi} - U_{sL})L}{E_{si}}] \qquad (16)$$

The solids concentration at the top of the column have been reported to be larger than the solids concentration in the effluent [Kato et al. (1972), and Smith and Ruether (1984)]. The boundary conditions at the top of the column

are difficult to describe because of the sudden change in gravity that the particles experience as they leave the column. The solids concentration above the top of the column is assumed to be uniform and equal to the concentration of the effluent. The relationship between the concentration of solids in the effluent and the concentration of solids at the top of the column may be expressed as:

$$C_{si}^{1} = \left[1 + \frac{\bar{\psi}_L U_{pi}}{(E_{si}/L) + U_{sL}}\right] C_{si}^{f} \qquad (17)$$

Here, the terminal particle velocity is used to represent the slip velocity of solids at the top of the column. The solids dispersion coefficient is obtained from Equation (15). Figure 7 shows the experimental value of C_{si}^{1} compared to the prediction of C_{si}^{1} from Equation (17). The average absolute relative error between observed and predicted solids concentration at the top of the column is 9.2 percent for all experimental conditions.

Effect of Independent Operating Variables

The effect of gas velocity on the axial solids concentration distribution is shown in Figure 8 for a binary particle system. Increasing gas velocity decreases the variance of the axial solids concentration distribution especially near the bottom of the column. In a similar manner, Figure 9 shows that increasing slurry velocity decreases the variance of the axial solids concentration distribution especially at the highest slurry velocity of 0.018 m/s. Figure 10 compares the axial solids concentration distribution for binary and ternary particle size mixtures. Here, the axial

solids concentration distribution is remarkably similar to both particle mixtures. The volumetric mean particle diameter of the slurry feed for the binary and ternary mixtures of solids is 55 μm and 65 μm, respectively. For the binary mixture of solids, the large particle tends to concentrate in the slurry bubble column, whereas, for the ternary mixture of solids more of the larger particles are in the slurry feed and the medium and small sized particles are more concentrated in the slurry bubble column.

Figure 11 compares the axial solids concentration distribution obtained in monodispersed and binary solids systems. The monodispersed solids are either 48.5 μm diameter particles or 193.5 μm diameter particles and the binary solids mixture consists of equal weight fractions of 48.5 μm diameter and 193.5 μm diameter particles. The axial solids concentration distribution for the binary mixture of solids between the larger monodispersed particle size concentration distribution and the smaller monodispersed particle size concentration distribution. Prediction of the axial solids distribution for the binary mixture can be made by averaging the sum of the axial solids concentration distribution for the monodispersed particle systems as is shown by the dashed line in Figure 11. Very good agreement is obtained between the observed and predicted axial solids concentration distribution for the binary particle size mixture which indicates that Equation (7) is valid for polydispersed systems.

Discussion

The prediction of the axial solids concentration distribution for polydispersed solids can be made by combining Equations (6a) or (6b) with Equa-

tion (7). The parameters U_{pi}, E_{si}, C_{si}^{1} are empirically correlated with Equations (14), (15) and (17). The gas holdup for a single component liquid and a perforated plate distributor may be calculated from Equation (13). The procedure for calculation of the axial solids concentration distribution for polydispersed solids is given in Figure 12. In addition to the above mentioned parameter estimations, the average solids concentration of the i^{th} particle size fraction, $\bar{C}_{si}$, is required to calculate the parameter $\bar{\psi}_L$. $\bar{C}_{si}$ is obtained from integration of Equation (6b).

$$\bar{C}_{si} = [(\bar{C}_{si}^{1} + \gamma_i)/B_i][\exp(-B_i)-1] - \gamma_i \qquad (18)$$

where:

$$B_i = -(\bar{\psi}_L U_{pi} - U_{sL})L/E_{si}$$

$$\gamma_i = U_{sL}C_{si}^{f}/(\bar{\psi}_L U_{pi} - U_{sL})$$

A comparison of the measured and predicted axial solids concentration distribution is given in Figure 13. The larger particles are seen to have the greatest influence on solids concentration near the bottom of the column whereas the smaller particles constitute a greater fraction of the solids near the top of the column. The total axial solids concentration distribution is reasonably well described by the sedimentation-dispersion model for polydispersed solids systems.

Conclusions

1. The sedimentation-dispersion model has been applied to polydispersed solids systems in a slurry bubble column and can be used to predict the axial solids concentration distribution as well as the particle size fraction distribution as a function of axial position.

2. No effects of particle-particle interaction from a particle size distribution was observed on the hindered settling velocity, U_{pi}, or the solids dispersion coefficient, E_{si}, of the i^{th} narrow-sized particle fraction.

Notation

B_I = parameter defined in Equation (18)

C_s = total solids concentration as a function of axial position, kg/m^3

C_s^f = total solids concentration of slurry feed, kg/m^3

C_{si} = solids concentration of i^{th} particle size fraction, kg/m^3

C_{si}^f = solids concentration of i^{th} particle size fraction in slurry feed, kg/m^3

C_{si}^o = solids concentration at bottom of column for i^{th} particle size fraction, kg/m^3

C_{si}^1 = solids concentration at top of column for i^{th} particle size fraction, kg/m^3

C_1 = constant defined by Equation (4), kg/m^3

C_2 = constant defined by Equation (5a) or (5b), kg/m^3

D = column diameter, m

d_{pi} = particle size of i^{th} particle size fraction, m

E_s = solids dispersion coefficient for monodispersed solids system, m^2/s

E_{si} = solids dispersion coefficient for i^{th} particle size fraction, m^2/s

F = objective function defined by Equation (12)

Fr_g = Froude number of gas phase

L = length of slurry bubble column, m

Pe_{pi} = solids Peclet number of i^{th} particle size fraction

Re_g = Reynolds number of gas phase

Re_{pi} = particle Reynolds number of i^{th} particle size fraction

$\tilde{U}_g$ = superficial gas velocity, m/s

U_p = hindered settling velocity for monodispersed solids, m/s

U_{pi} = hindered settling velocity for i^{th} particle size fraction, m/s

U_{sL} = slurry velocity, m/s

$\tilde{U}_{sL}$ = superficial slurry velocity, m/s

U_{ti} = terminal settling velocity of i^{th} particle size fraction, m/s

X = dimensionless axial position

Z = height from bottom of column, m

Greek Symbols

γ_i = parameter defined in Equation (13), kg/m^3

ε_g = gas holdup

μ_l = liquid velocity, Pa-s

ρ_L = liquid velocity, kg/m^3

σ_L = liquid surface tension, N/M

$\bar{\psi}_L$ = average fraction of liquid in slurry

References

Ahrendts, J., and Baehr, H., "The Use of Nonlinear Regression Analysis in Establishing Thermodynamic Equations of State," Int. Chem. Eng., 21, p. 572 (1981).

Akita, K., and Yoshida, G., "Gas Holdup and Volumetric Mass Transfer Coefficient in Bubble Columns," Ind. Eng. Chem., Process Des. Develop., 12, p. 76 (1973).

Chaudhari, R.Y., and Ramachandran, P.A., "Three Phase Slurry Reactors," AIChE, J., 26, p. 177 (1980).

Cova, D.R., "Catalyst Suspension in Gas-Agitated Tubular Reactors," Ind. Eng. Chem., Process Des. Develop., 5, p. 20 (1966).

Hikita, H., Asai, S., Tanigawa, K., Segawa, K., and Kitao, M., "Gas Holdup in Bubble Columns," Chem. Eng. J., 20, p. 59 (1980).

Hughmark, G.A., "Holdup and Mass Transfer in Bubble Columns," Ind. Eng. Chem., Process Des. Develop., 6, p. 218 (1967).

Kato, Y., Nishiwaki, A., Fukuda, T., and Tanaka, S., "The Behavior of Suspended Solid Particles and Liquid in Bubble Columns," J. Chem. Eng. Japan, 5, p. 14 (1972).

L'Homme, G.A., "Introduction to the Applied Physical Chemistry and Chemical Engineering Problems Raised by Gas-Liquid-Solid Catalyst Reactions and Reactors," Chemical Engineering of Gas-Liquid-Solid Catalyst Reactions, ed. G.A. L'Homme, CEBEDOC., Liége (1979).

Reilly, I.G., Scott, D.S., and Abou-El-Hassan, M., "Leaching in a Bubble Column Slurry Reactor," Can. J. Chem. Eng., 60, p. 399 (1982).

Smith, D.N., and Ruether, J.A., "Dispersed Solids Dynamics in a Slurry Bubble Column," accepted in Chem. Eng. Sci. (1984).

Suganuma, T., and Yamanishi, T., "Behavior of Solid Particles in Bubble Columns," Kagaku Kogaku, 30, p. 1136 (1966).

Yamanaka, Y., Sekizawa, T., and Kubota, H., "Age Distributions of Suspended Solid Particles in a Bubble Column," J. Chem. Eng. Japan, 3, p. 264 (1970).

TABLE 1. Experimental Conditions for Present Investigation

Slurry Velocity	Polydispersed Solids Systems*				
m/s	1	2	3	4	5
0.0075	A_1, B_1, C_1	A_1, C_1		B_2, C_2	
0.012			A_1, C_1		
0.018					A_1, B_1, C_1

Symbol: Mean particle size of narrow-sized fraction, μm

A	48.5
B	96.5
C	193.5

Subscripts: Particle density, kg/m^3

1	2420
2	3990

*All solids systems were run at four gas velocities: 0.031-, 0.089-, 0.152-, and 0.200-m/s. Each solid system contained equal mass fractions of narrow-sized particles.

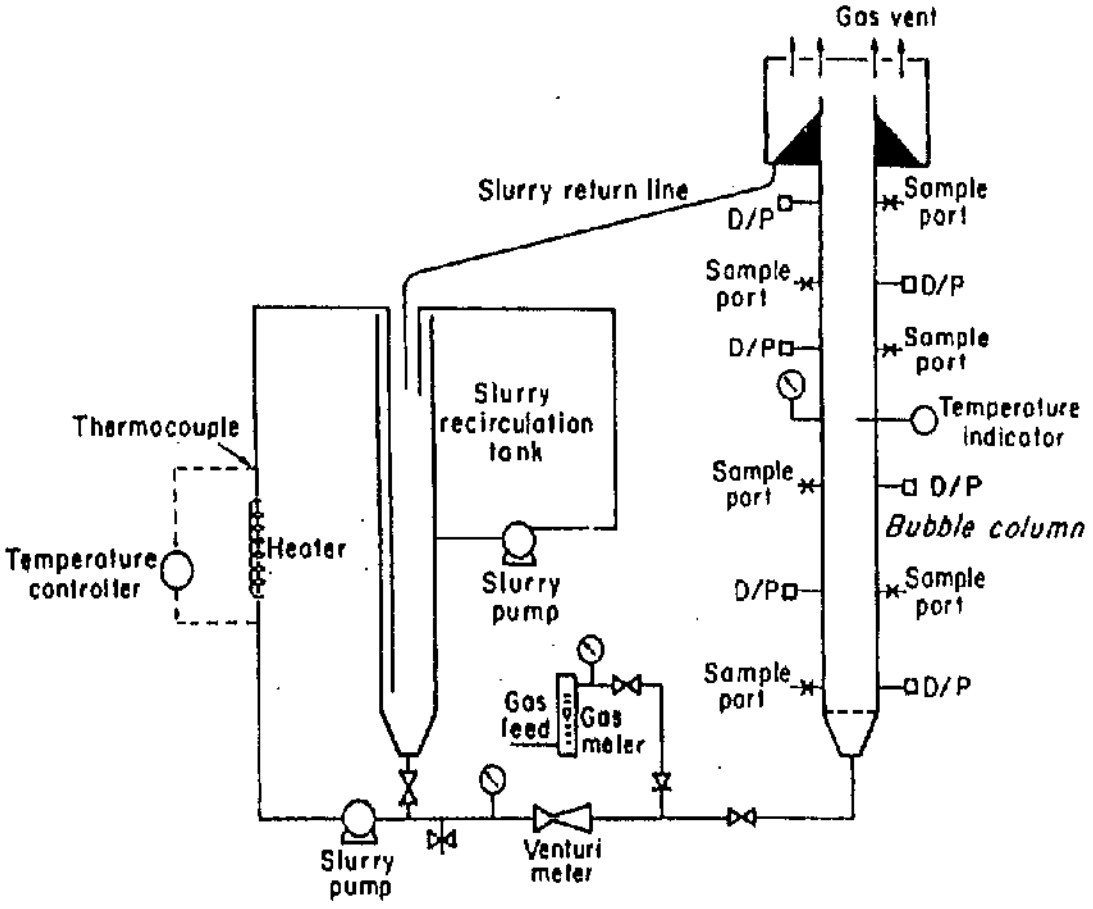

1-13-81 L-18107

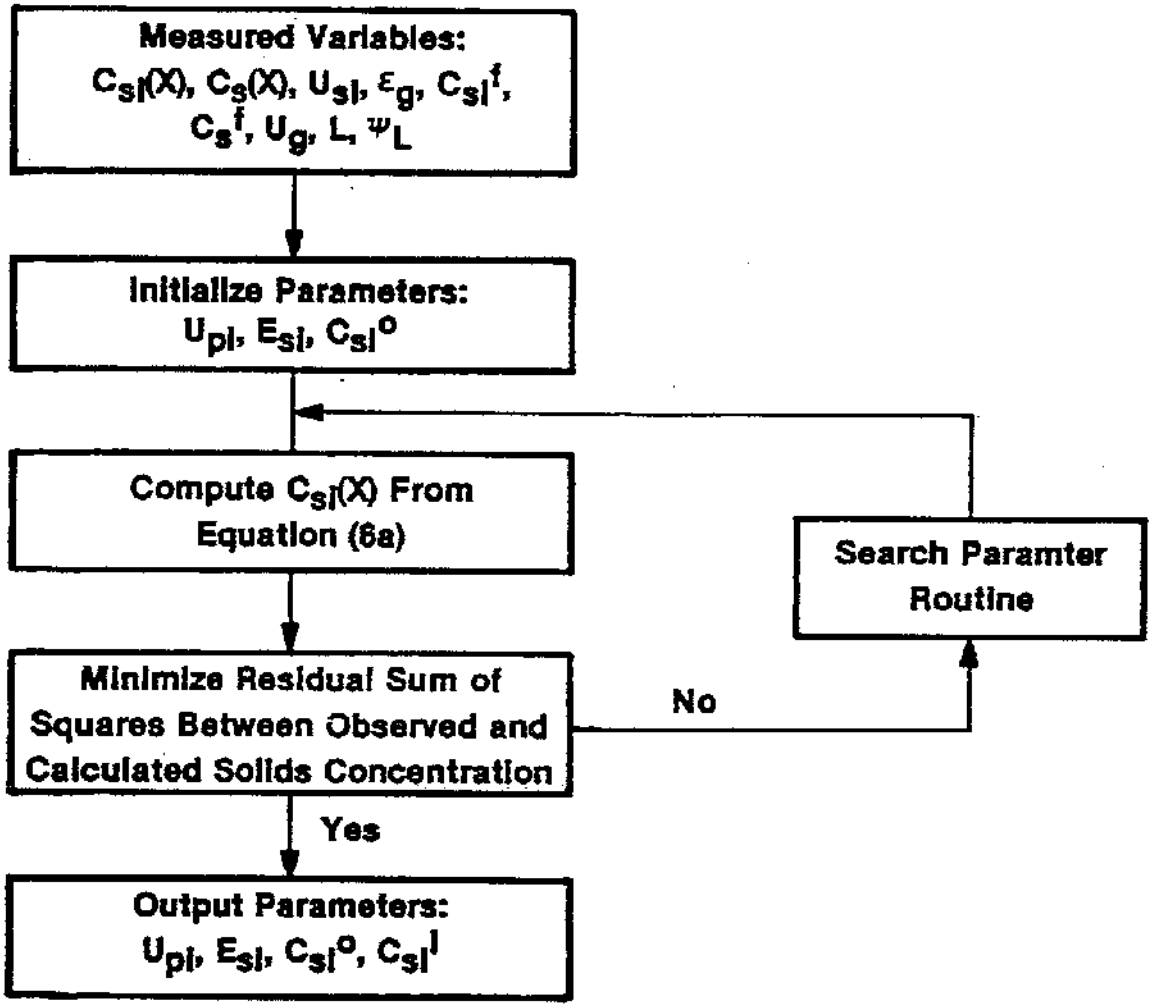

Figure 2. Analysis of Measured Axial Solids Concentration Distributions.

BSI/5824

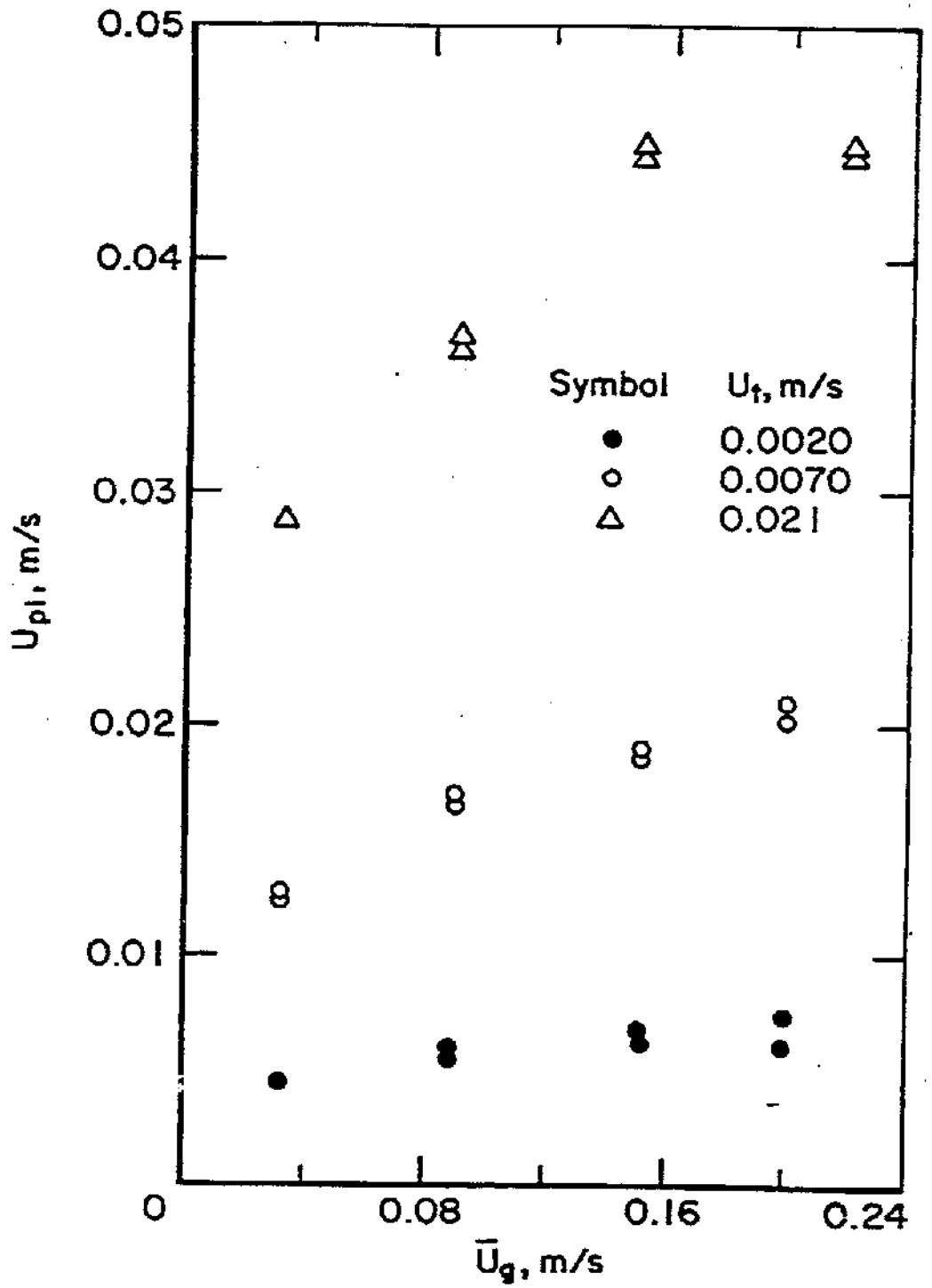

Figure 3 - Effect of gas velocity on hindered settling velocity.

BSU/5826

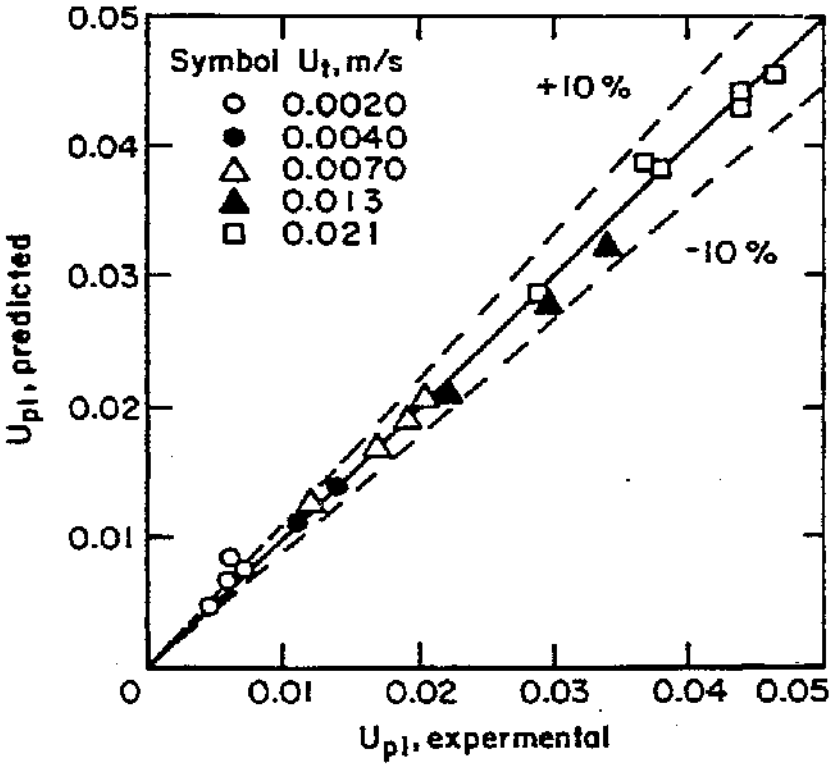

Figure 4 - Parity plot of observed hindered settling velocity and hindered settling velocity predicted from equation (14).

BSI/5835

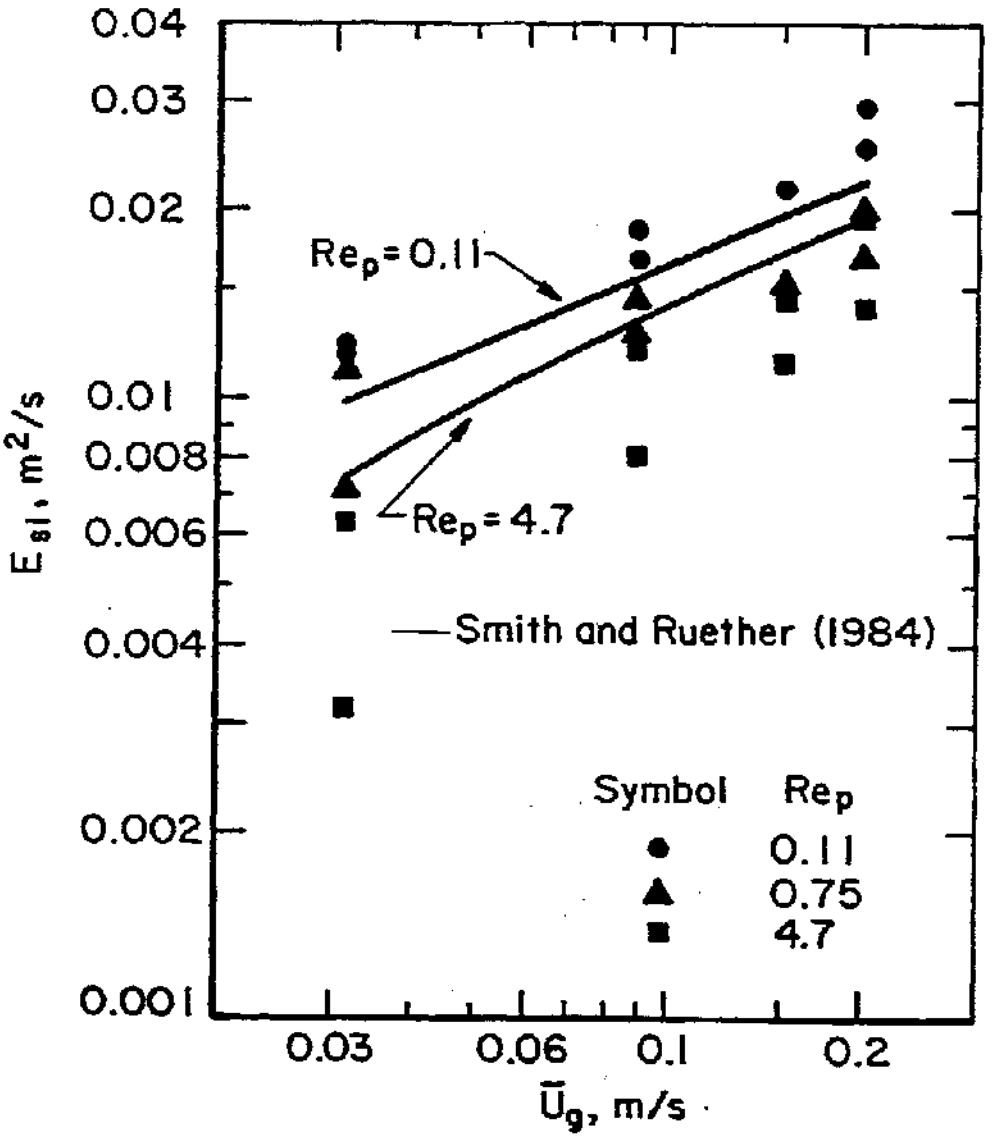

Figure 5 - Effect of gas velocity on solids dispersion coefficient.

BSI/5827

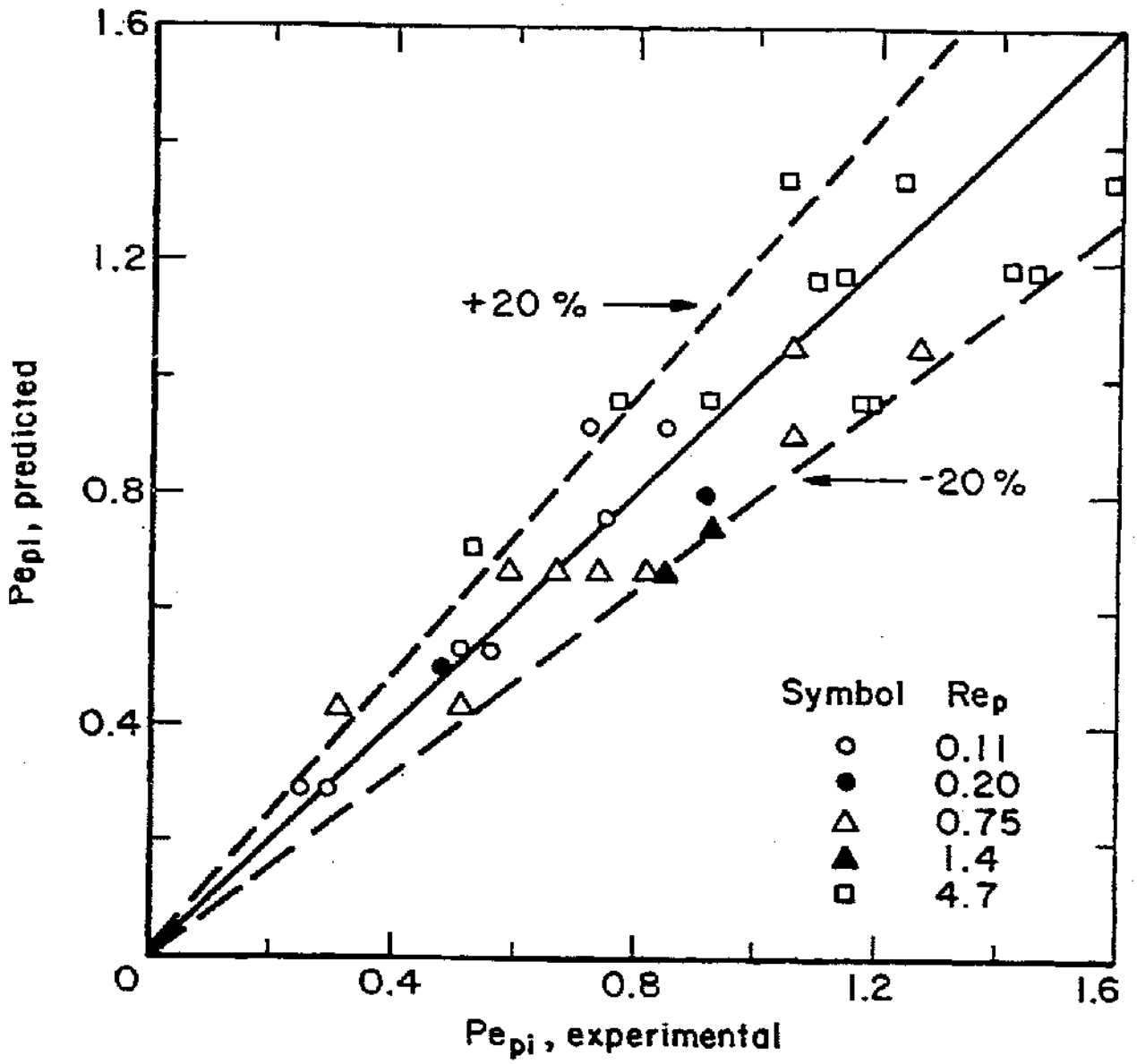

Figure 6 - Parity plot of experimental solids Peclet number and solids Peclet number predicted from Equation (15).

BSI/5828

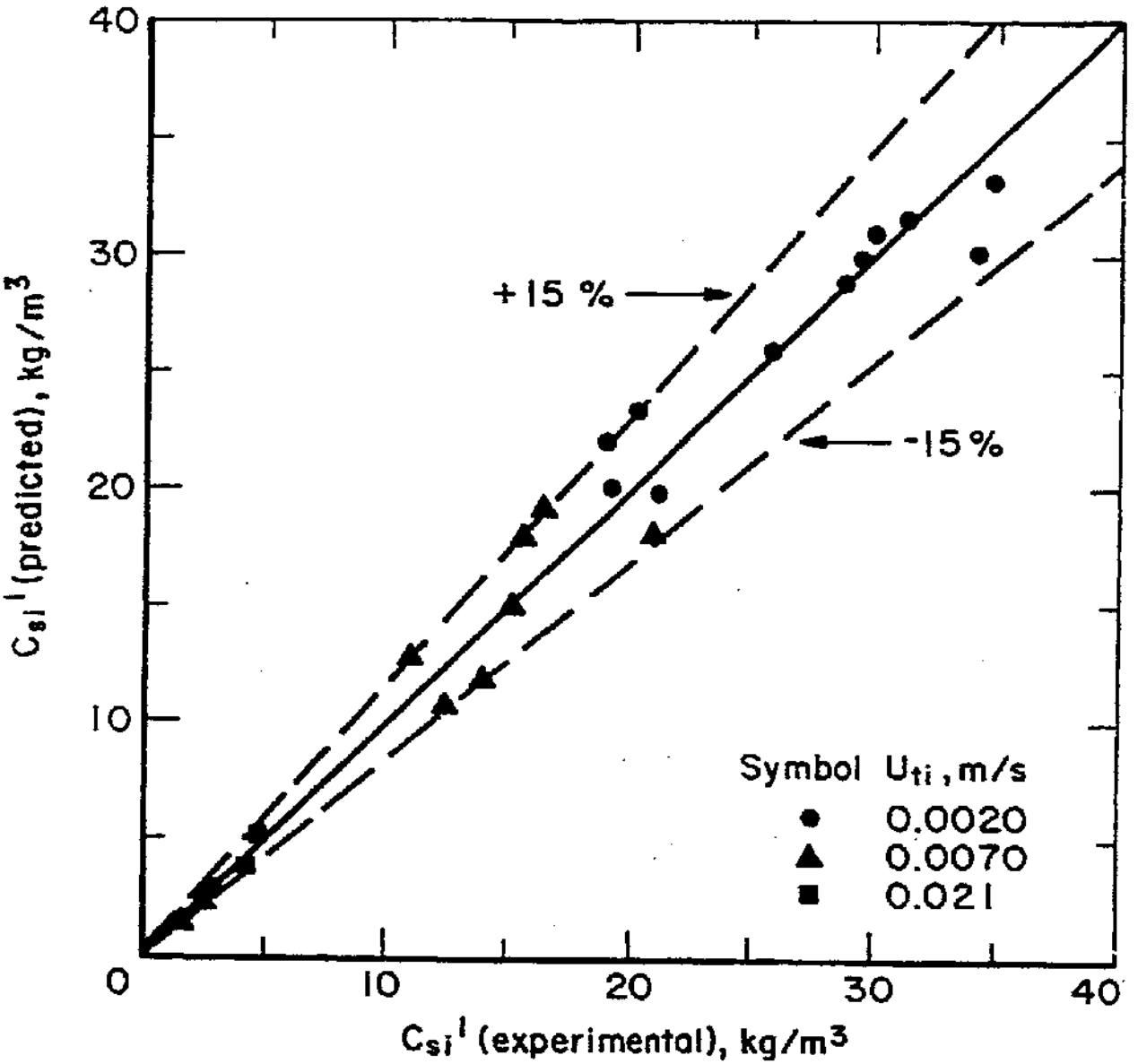

Figure 7 - Parity plot of experimental solids concentration at the top of the column and that predicted from Equation (17).

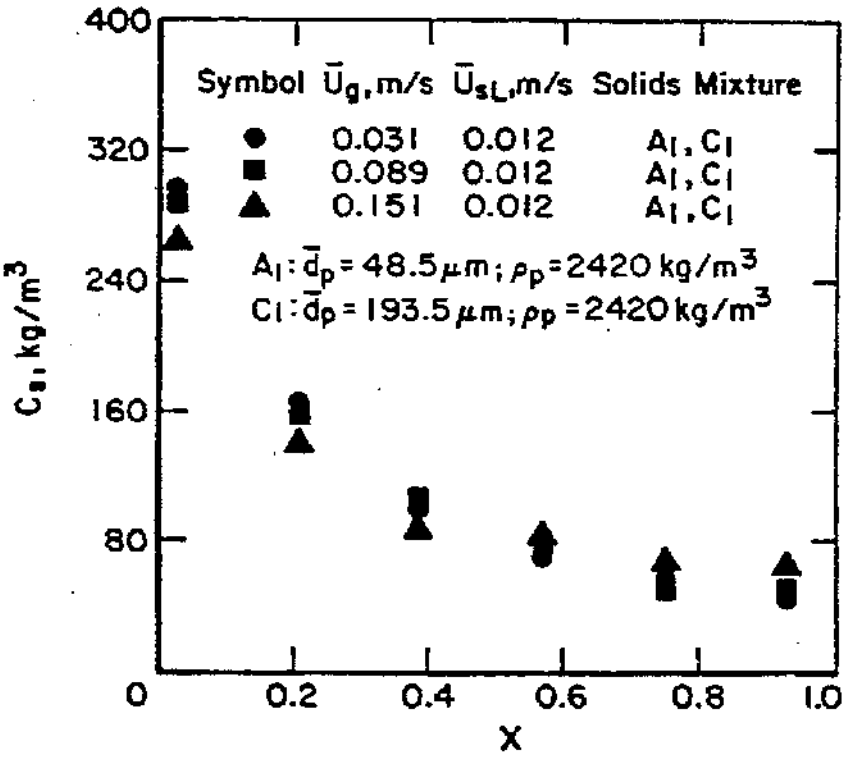

Figure 8 - Effect of gas velocity on axial solids concentration distribution for poly-dispersed solids system.

BSI/5830

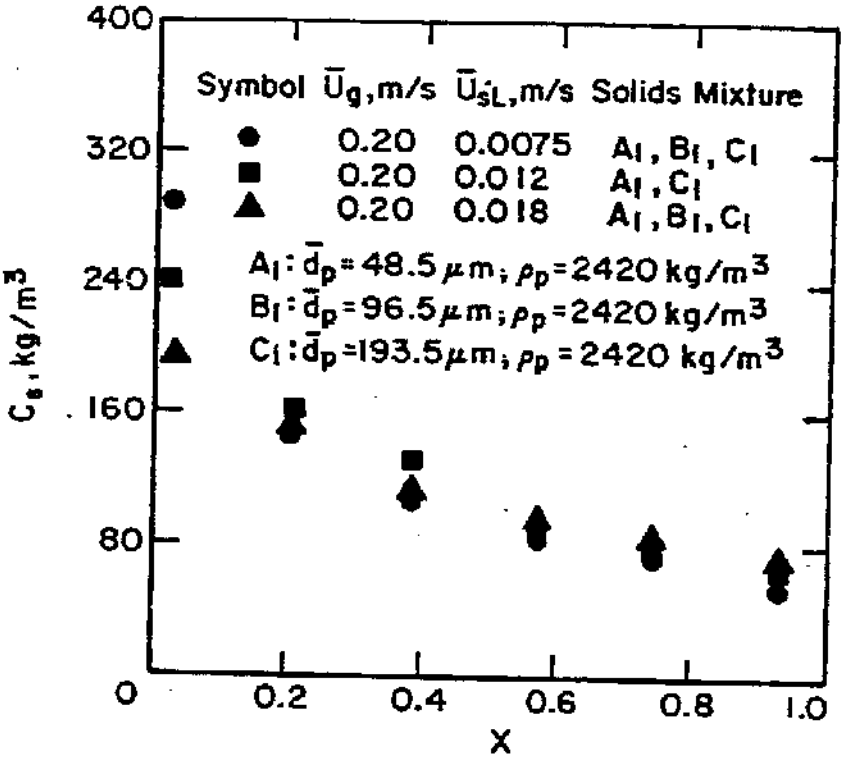

Figure 9 - Effect of slurry velocity on axial solids concentration distribution in polydispersed solids system.

BSI/5832

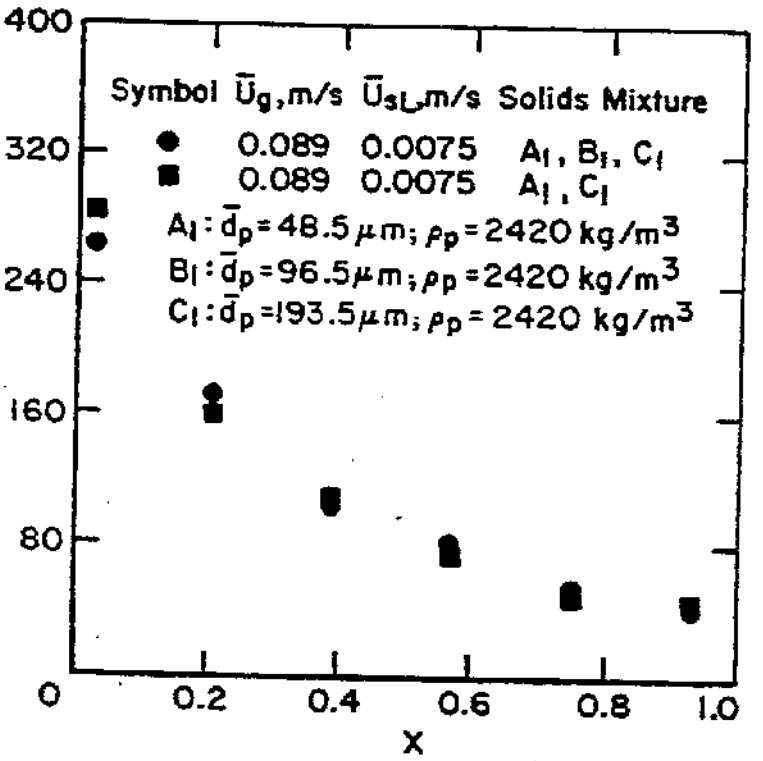

Figure 10- Comparison of axial solids concentration distribution for binary and ternary mixtures of partical size.

BSI/5831

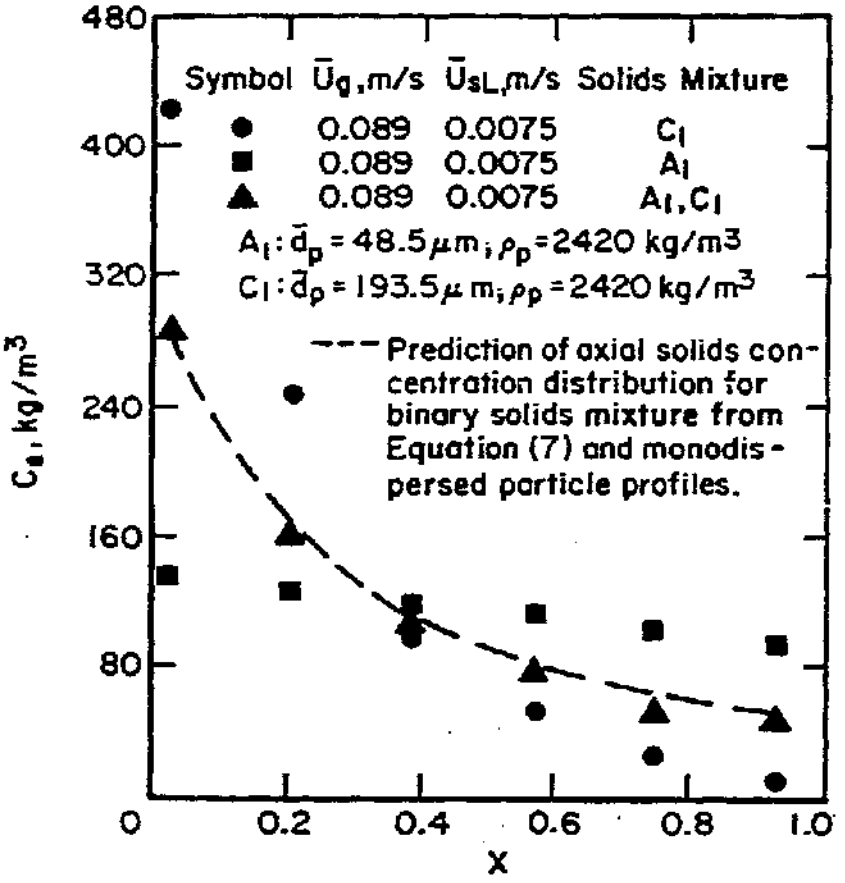

Figure 11- Comparison of axial solids concentration distribution for monodispersed particles and a binary mixture of particle size.

BSI/5833

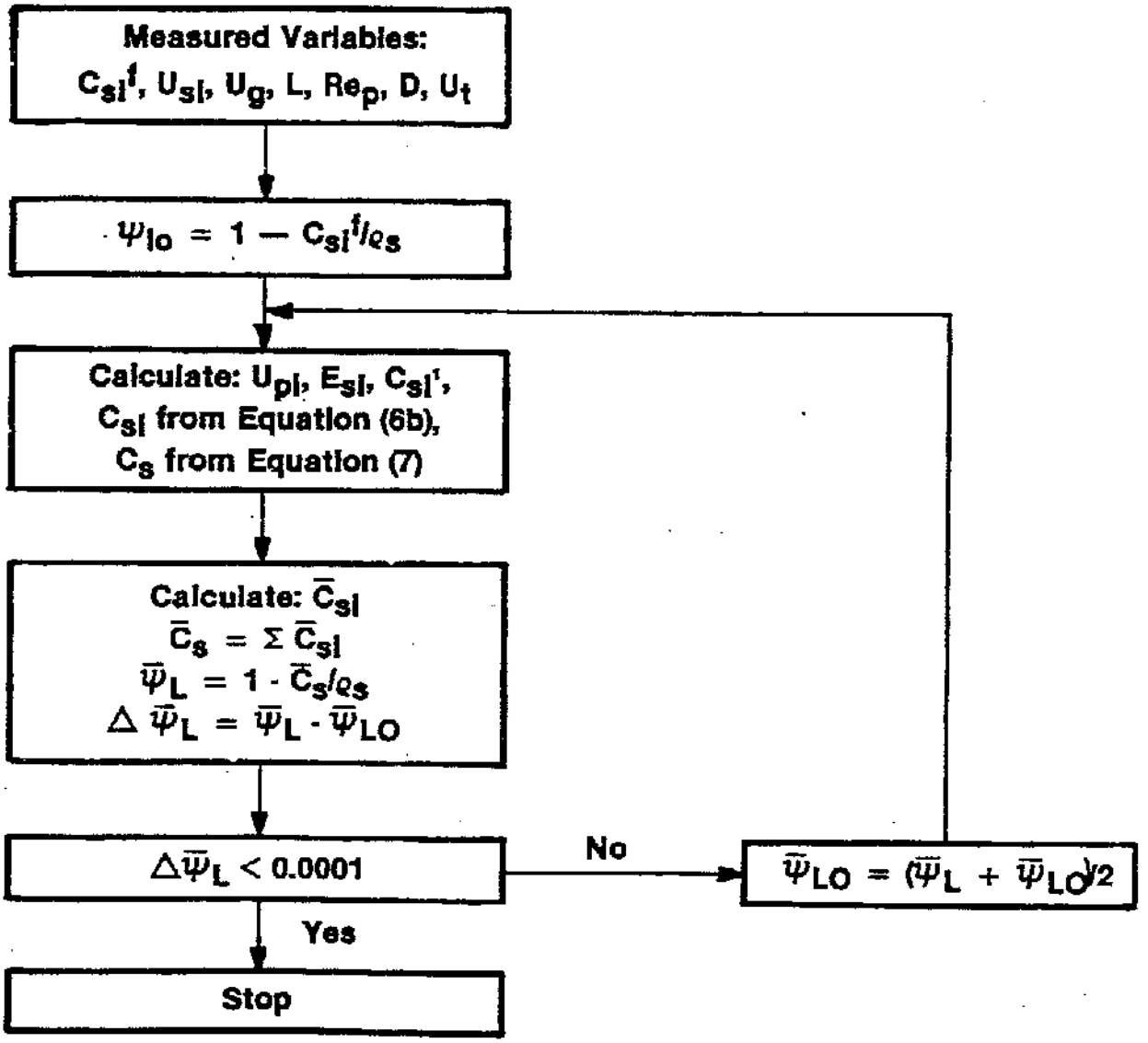

Figure 12. Procedure for Calculation of Axial Solids Concentration Distribution for Polydispensed Solids Systems.

BSI/5825

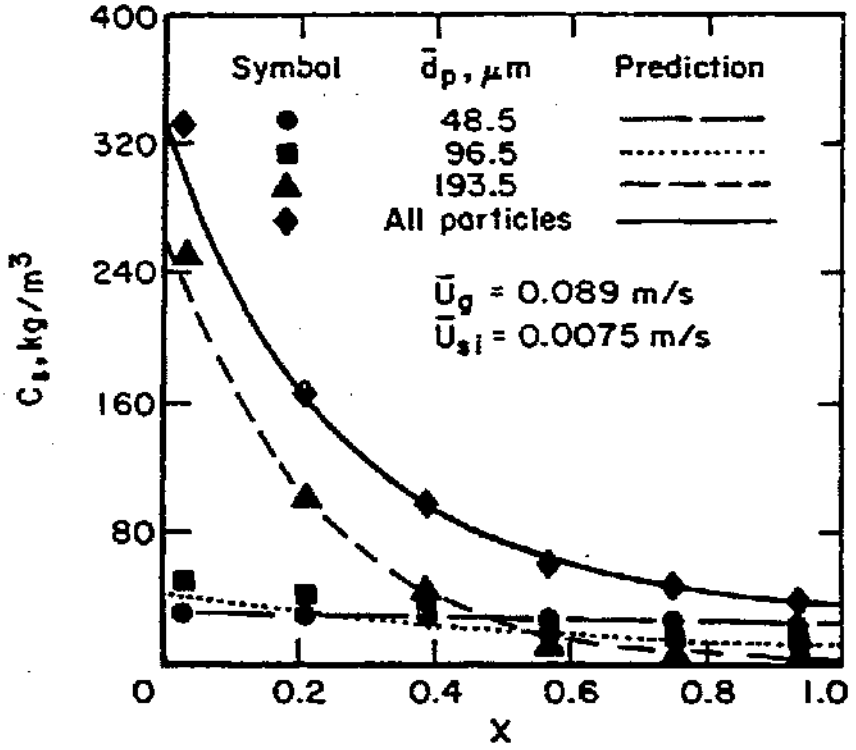

Figure 13 - Comparison of observed and predicted axial solids concentration distribution for polydispersed solids system.

BSU/5834